



Discrimination of invasive ductal and lobular carcinoma of the breast based on the combination of enhanced Legendre polynomial, kinetic features and deep learning features

Ali M. Hasan ^{a,*}, Noor K.N. Al-Waely ^a, Hadeel K. Aljobouri ^b, Hamid A. Jalab ^c, Rabha W. Ibrahim ^c, Farid Meziane ^d

^a College of Medicine Al-Nahrain University Baghdad Iraq

^b Department of Biomedical Engineering College of Engineering Al-Nahrain University Iraq

^c Information and Communication Technology Research Group, Scientific Research Center, Al-Ayen University, Nile Street 64001 Thi-Qar, Iraq

^d Data Science Research Centre, School of Computing, University of Derby, United Kingdom



ARTICLE INFO

Keywords:

Breast cancer

ILC

IDC

ELP

Kinetic features

Deep learning

ABSTRACT

The fifth most common cause of cancer-related deaths among women worldwide is breast cancer, which is the most common cancer among women globally. Early detection of breast cancer through regular screenings and awareness of symptoms can lead to better prognosis and more effective treatment options. Breast cancer is a diverse disease that comes in more than 20 varieties. It is generally divided into two categories based on histology: in-situ carcinoma and invasive (infiltrating) carcinoma. These categories are further divided into four subcategories based on the location of the tumor's origin: invasive ductal carcinoma (IDC), invasive lobular carcinoma (ILC), lobular carcinoma in situ (LCIS), and ductal carcinoma in situ (DCIS). The aim of this study is to use medical image processing and machine learning to accurately diagnose invasive lobular carcinoma (ILC) and invasive and lobular carcinoma (IDC) of the breast. This study develops a novel hybrid feature extraction model to improve the diagnosis accuracy of breast cancer. Deep learning, kinetic, and enhanced Legendre polynomial features have been combined to create a hybrid feature model that enhances IDC and ILC discrimination. The proposed model consists of four stages: data collection, preprocessing, feature extraction, and classification. The publicly available DCE-MRI dataset was used in this study, and the results showed classification accuracy of 97.99% in combined post-contrast-1 model. Overall, the results demonstrated the benefits of the hybrid feature extraction model and the fact that this study is non-invasive, uses only medical image processing, and does not require biopsies to enhance treatments.

1. Introduction

Breast cancer is the world's most prevalent cancer and the fifth leading cause of death among women globally. In 2020, about 2.3 million females were diagnosed with breast cancer which accounted for 11.7 % of the global cancer incidence [1]. While, according to the Iraqi Ministry of Health, breast cancer represents the main cause of mortality among women in Iraq and accounts for about one-third of all recorded cases in 2019 [2]. Thus, the Iraqi Ministry of Health has launched, in cooperation with the World Health Organization (WHO), a nationwide program for early diagnosis and down staging of breast cancer since

2000 by building several specialist clinics, spread across the governorates of Iraq [3]. Where, WHO reported that early detection of breast cancer while it is still small, may reduce the death rates and provide the best chance of effective treatment for women with the breast cancer [4].

The female breast anatomy is formed from several types of tissues: glandular, connective or fibrous, and fatty. Where, the glandular tissue of the mammary glands includes branching ducts and the terminal secretory lobules. There are about 15–20 lobes which comprise a set of smaller lobules which produce milk and drain it into a network of breast ducts within the breast tissue. These ducts converge toward the nipple. The connective, also known as fibrous or supportive tissue, is

* Corresponding author.

E-mail addresses: aialwaeli@nahrainuniv.edu.iq (A.M. Hasan), noor83kadhem@nahrainuniv.edu.iq (N.K.N. Al-Waely), hadeel.k.aljobouri@nahrainuniv.edu.iq (H.K. Aljobouri), hamid.a@alayen.edu.iq (H.A. Jalab), rabha@alayen.edu.iq (R.W. Ibrahim), F.Meziane@derby.ac.uk (F. Meziane).

responsible for holding glandular and fatty tissue in place. Finally, fatty tissue fills in the space between glandular and supportive tissue, and determine the breast size, as shown in Fig. 1 [5]. Breast cancer begins as a growth of some breast cells in any part of the breast, including the ducts, lobules, and connective tissue, faster than the healthy ones.

Consequently, a lump or mass of tissue is formed from an accumulation of abnormal cells. Breast cancer can invade and grow into the surrounding tissue of the breast such as lymph nodes or travel through the blood stream to other parts of the body [6]. Breast cancers are classified as invasive meaning that they can spread beyond their original site and into the surrounding tissues. Histological type and grade of breast carcinoma are indispensable determinants of tumor management and prognosis [7]. Breast cancer is a heterogeneous disease, and more than 20 types of breast cancer are broadly classified histologically into *in-situ* carcinoma and invasive (infiltrating) carcinoma, which are classified furthermore based on the site from which the tumor originated into Ductal Carcinoma in Situ (DCIS), Lobular Carcinoma in Situ (LCIS), Invasive Ductal Carcinoma (IDC), and Invasive Lobular Carcinoma (ILC) [8,9]. Ductal Carcinoma in Situ (DCIS) and Invasive Ductal Carcinoma (IDC) begin forming in the milk ducts and may spread beyond the ducts to the other parts of the breast tissue. They are the most common type of breast cancer, and account for approximately 40–75 % of all invasive breast cancer incidence, according to the American Cancer Society [10]. Lobular Carcinoma in Situ (LCIS) and Invasive Lobular Carcinoma (ILC) begin in lobules and have distinct biological characteristics by distinct cell configurations that distinguish them from ductal carcinoma. They are the second most common type of breast cancer, and account for approximately 5–15 % of all invasive breast cancer [11]. Fig. 2 shows T1 weighted images of two women with invasive ductal carcinoma and invasive lobular carcinoma. Moreover, the diffused growth patterns exhibit a slight perturbation of the normal tissue architecture, rendering it more difficult to identify through manual breast examination and clinical breast imaging methods [8,9,12,13].

Early detection of breast cancer followed by suitable treatments has the potential to decrease breast cancer death rates significantly in the long-term, and give the best prognosis [14]. Currently, the mammogram is a common standard breast screening technique that uses low-dose

20–30 KeV x-rays to examine breast. However, there is a set of limitations and side effects of utilizing mammographic imaging. Interpretations of mammograms can be difficult because a normal breast looks different for each woman, as well as, some of breast cancers are hard to visualize by mammogram especially for women under 40 years old [14]. Furthermore, the mammogram is greatly sensitive to the breast tissue density. So, the mammograms of young women who have a dense breast, can be harder to read than the mammograms of older women who have a fatty breast, as shown in Fig. 3. Because there is more glandular tissue in young women, the mammogram's overall sensitivity drops to as low as 30 % to 48 %, while it still has a sensitivity of 75 % to 85 % in fatty breast tissue [15]. Moreover, exposed to x-rays can lead to various harmful biological and health effects, such as DNA mutation, and cell damage, resulting in increasing breast cancer incidence rates [4]. Additionally, the mammogram is unreliable in distinguishing between benign and malignant tumors precisely [16]. Therefore, other breast imaging techniques are needed such as ultrasonography (US) and magnetic resonance imaging (MRI). US is a non-invasive imaging modality that uses sound waves of 1–12 MHz frequency to reflect off at the boundaries of internal body structures [8].

It can be employed as a supplementary technique in conjunction with other imaging modalities for diagnosing some breast lesions that are indistinguishable in mammogram due to breast density [18,19]. Additionally, US cannot always detect whether a growth is benign or cancerous due to sonographic characteristics overlapping [4]. Therefore, US can be used instead as a supplementary technique in conjunction with other imaging modalities [1,6,15,19]. The third imaging modality is magnetic resonance imaging (MRI), it is a non-invasive screening imaging technique that creates a set of different cross-sectional scans by applying strong magnetic field with radio frequency (RF) signals [15,20]. However, MRI is relatively the most expensive compared to other breast cancer detection modalities [21]. Modern MRI scanners produce a set of sequences that are categorized according to the particular appearance of tissues. The standard breast MRI examination incorporate multiple pulse sequences, typically including the following sequences at minimum; (i) T2-weighted imaging, which is routinely performed, and (ii) dynamic T1-weighted contrast-enhanced sequences (DCE-MRI) before and after contrast injection. The former sequence is usually obtained at the start of the exam. Breast masses with high signal intensity at T2-weighted imaging include high water content such as cyst and lymph nodes [4]. In clinical practice, T2-weighted sequence is always considered as a complementary sequence to DCE-MRI breast findings [22]. Therefore, the corner stone in breast pathology diagnosis is the DCE-MRI, which includes performing T1-weighted imaging prior and after intravenous administration to show enhancing abnormalities. Where, the repetitive MRI scan which is known by post-contrast dynamic T1 weighted sequences, starts after administrating gadolinium compound through intravenous injection by approximately (60–90 s). At this time, the gadolinium material decreases the relaxation time of water protons, resulting in making most of breast cancers to become hyperintense within the initial upslope phase which usually takes 2 min [23]. Then the initial upslope phase is followed by a delayed phase which includes three distinct forms of signal intensity of the suspicious lesions, or also known by kinetic curves; Type 1 (persistent curve) shows a progressive increase in the signal intensity on each successive post-contrast dynamic T1 weighted sequences over time. Whereas, if the signal intensity remains steady on each successive contrast-enhanced scans, this pattern is called Type 2 (plateau curve). However, if the signal intensity drops off significantly on the successive contrast-enhanced scans, this pattern is called Type 3 (washout curve).

Several studies have reported that kinetic curves provide high sensitivity and low specificity in diagnosing benign and malignant breast lesions [6,24]. The decision of which method to use is influenced by the characteristics of the mass as well as the patient's breast tissue [25,26]. However, the pathological examination is based essentially on the experience of the pathologists to analyze the characteristics of the

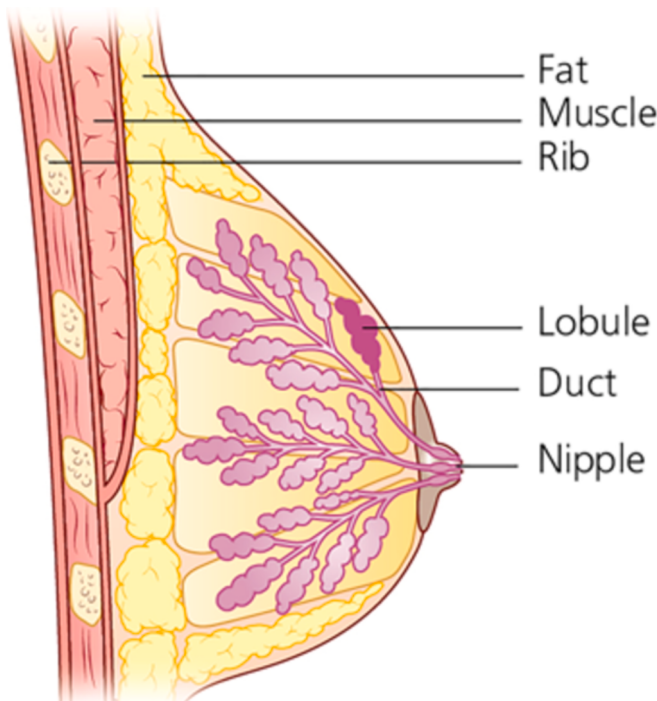


Fig. 1. Anatomy of the breast [4].

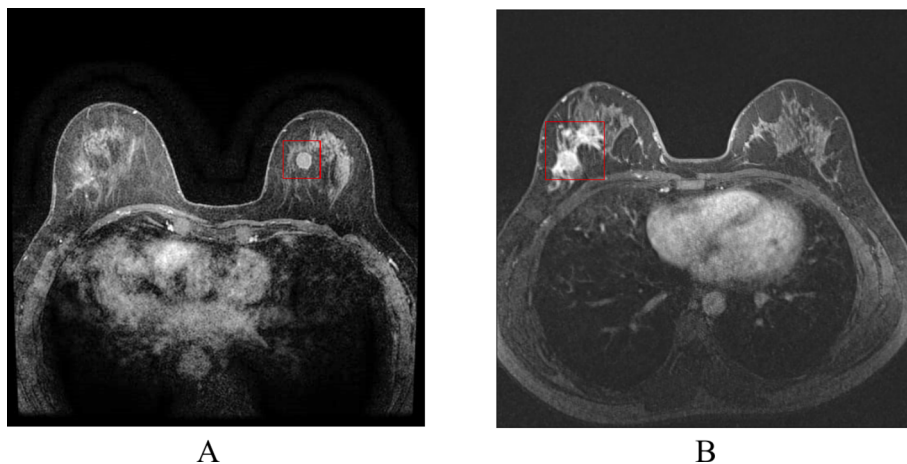


Fig. 2. T1 weighted images of two women with malignant breast lesion inside the red rectangles. A) Invasive lobular Carcinoma, and B) Invasive ductal carcinoma.

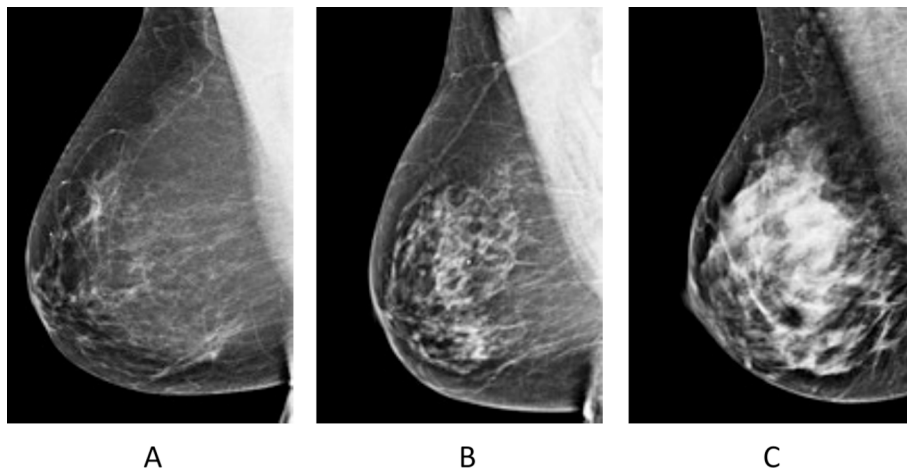


Fig. 3. The mammogram of a range of breast density. A) Fatty breast, B) Some breast density, and C) Dense breast [17].

lesions through tissue sections staining. Therefore, it is susceptible to human error, including misidentification of tissue features, misinterpretation of cellular characteristics, and fatigue-induced mistakes. Even experienced pathologists can make errors, which can affect the accuracy of diagnoses. Furthermore, manual examination requires considerable time and effort, especially for complex or ambiguous cases. This can lead to delays in diagnosis and treatment initiation, potentially impacting patient outcomes, particularly in cases where rapid intervention is necessary [4,6,8].

2. Related work

Recently, there have been several studies on utilizing breast DCE-MRI data that have exploited the vital role of kinetic models to predict breast masses histopathological classification into ductal and lobular carcinoma. Maiti, Nayak [27] investigated the performance of the radiomic features (RF) which were extracted from DCE-MRI for differentiating IDC from ILC cancers. The RF features were extracted from DCE-MRI sequences using a 3D slices, and included the following feature sets; shape feature, gray level dependence matrix (GLDM), gray level co-occurrence matrix (GLCM), First order, gray level run length matrix (GLRLM), gray level size zone matrix (GLSZM), and neighboring gray tone difference matrix (NGTDM). The maximum achieved area under curve (AUC), sensitivity, and specificity was 0.998, 97.21 %, and 96.2 % respectively on classifying a dataset that included 58 patients (30 with IDC and 28 with ILC), and downloaded from Duke University Hospital in

USA [28]. Faraz, Daunce [29] extracted the radiomics features; included GLCM, GLRLM, NGTDM, and GLSZM from three MRI image types (DCE-MRI, subtraction, and T2-weighted images) to discriminate histological subtypes such as IDC and ILC cancers. The maximum achieved AUC was 0.73 when using the support vector machine (SVM) classifier to classify a dataset that included 420 MR images of breast cancer from 323 patients. Conte, Tafuri [30] proposed an automated system that included two main consecutive subsystems. The first one was the ROI Hunter, which was used to localize the tumoral regions of interest (ROIs) automatically through an iterative procedure based on intensity value, followed by extracting deep features and classification. While the second one was used to discriminate between *in situ* and infiltrating breast tumors through extracting the radiomics features form the located the ROI. These features comprised shape, first order features, GLCM, GLRLM, GLDM and GLSZM. The maximum achieved ROC value was 0.7 of classifying 55 anonymized DCE-MRI sequences.

This study aims to utilize more diagnostic information from kinetic models in addition to pre-contrast and post-contrast MRI dynamics to classify the breast cancers automatically into ductal and lobular types thus reducing unnecessary breast biopsies. Determining which abnormalities are more likely to be cancerous and therefore requiring a biopsy is beneficial to reduce several risks that can be caused by biopsy such as infection and bleeding at the biopsy site. This study's primary contributions are:

1. To classify breast cancer in DCE-MRI scans, a novel feature extraction technique based on enhanced Legendre polynomial features

(ELP) is developed.

2. A CNN with four layers has been created specifically to extract deep features (DFs) from breast DCE-MRI sequences to increase the accuracy of the diagnosis.

3. A hybrid feature model that improves IDC and ILC discrimination has been created by combining three methods of feature extraction from DCE-MRI scans of the breast: deep learning, kinetic, and enhanced Legendre polynomial features.

3. Material and method

This study proposed a model that utilizes radiomic features that are extracted from DCE-MRI of the breast to optimize the diagnostic process of invasive ductal and lobular carcinoma of breast masses with reducing unnecessary follow-ups or biopsies. The proposed model consists of four stages: data collection, preprocessing, feature extraction, and classification, as depicted in Fig. 4.

3.1. DCE-MRI dataset

The DCE-MRI dataset used in this study was acquired between January 1, 2000, and March 23, 2014, and was downloaded from Duke University Medical Center in the United States [28]. The dataset consisted of 922 DCE-MRI breast sequences, all of which were obtained with a specialized four-channel breast array coil and a magnetic field strength of 1.5 T or 3 T using systems (GE Medical System and Siemens). Each breast MRI sequence included one T1-weighted alongside up to multiple T1-weighted DCE post-contrast sequences acquired after contrast agent injection, with a median of 117 s passed between post-contrast acquisitions. Additionally, most of these breast DCE-MRI sequences were malignant and chosen for this study, and the MR sequences with poor quality were excluded. The proposed model was trained with a total of 1095 malignant breast masses (616 IDC and 479 ILC) from 430 histopathological definitive DCE-MRI patients with a single lesion in either the left or right breast. Before extracting image features, a skilled radiologist manually delineated a region of interest (ROI) surrounding each DCE-MRI lesion to validate and authenticate the supplied annotations from the downloaded dataset.

3.2. DCE-MRI breast image preprocessing

Almost every MRI exam includes some kind of artifact that may reduce the quality of examinations. The artifacts may appear in MRI for a variety of sources that may be patient-related, signal processing-related, or MRI hardware fault [6]. Three primary categories of MRI artifacts can be distinguished: hardware and software artifacts, intrinsic physical artifacts, and physiologic artifacts. Physiologic artifacts are caused by motion or movement of the object being scanned including breathing, cardiac movement, and blood flow. Consequently, blurry,

ghostly, and stretchily MRI scans are produced due to this type of artifacts [31]. While inherent physics artifacts have occurred when the patient has an implant or metallic foreign bodies that are found in and on patients' bodies that respond to medical field and resulting to occur magnetic susceptibility artifacts. This creates bright or black areas at the edge of the magnetic object and may be misinterpreted as pathology. Finally, the hardware/ software artifacts occur when external magnetic field induction interferes with an MRI unit, gradient non-linearity, RF field non-uniformity, timing errors, a symmetrical brightness RF noise, and zero crossing line [32–34]. Additionally, non-standard variations in signal intensity between the same and consecutive MRI slices result from high dependence on the manufacturer, sequence type, and acquisition and reconstruction parameters of MRI scanners even though maintaining these MRI parameters consistent across different scanners [31,35,36]. Therefore, the elimination of MRI artifacts and intensity variations typically involves implementing a set of image preprocessing algorithms such as image enhancement, intensity normalization, and image registration. A Gaussian filter is used as a spatial domain filter that weight each pixel according to the neighborhood pixels and given variance value, to enhance the fine details of the breast DCE-MRI scan [10,37]. Furthermore, due to the Duke dataset being collected over a span of 14 years, this indicates that it was gathered using various imaging devices, pixel spacing, and spatial resolution, resulting in a large variability in image intensities among inter-patient and intra-patient acquisitions [36]. Thus, all breast DCE-MRI scans were normalized by histogram normalization algorithm to enhance the contrast in an image through the stretching out of its intensity range [1,10]. Finally, to standardize the spatial resolution of the downloaded dataset, through the use of bilinear interpolation, all breast DCE-MRI scans were registered to the same spatial resolution [1].

A region of interest (ROI) was placed on each breast lesion and cropped from all breast DCE-MRI slices by a radiologist with experience in diagnosing breast cancer in order to lessen the impact of confounding from the noncancerous voxels. The size of the region of interest (ROI) was determined by the longest diameter of each breast lesion, typically falling within the range of 20 to 30 pixels, adding a margin of 5 pixels around the lesion to include the parenchyma. The ROI was selected manually by the radiologist according to a set of criteria; the non-enhanced areas such as the edge of the breast lesions, formation of hemorrhagic, the microscopic cystic changes, necrotic areas inside the tumor, and vessels were avoided as much as possible due to have certain influence on the results. Finally, due to the recognized ROIs being not identical, all ROIs were resized by padding with zeros instead of rescaling because the deep learning method does not accept variation in the dimensions of the provided image.

3.3. Breast DCE-MRI feature extraction

The feature extraction algorithm aims to extract the most relevant

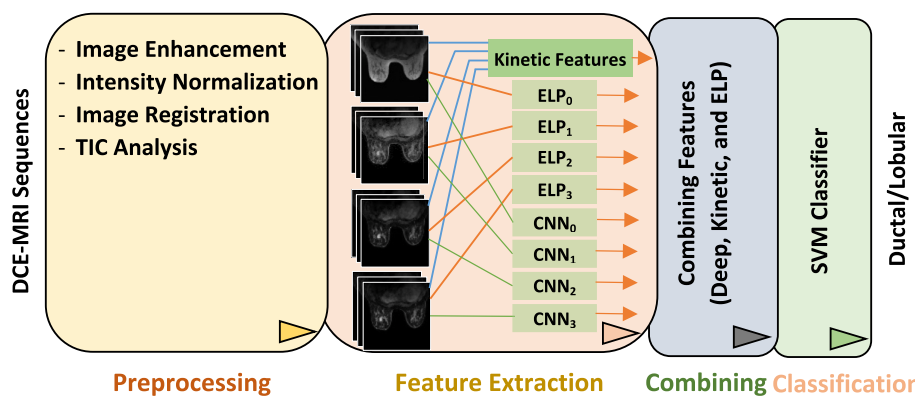


Fig. 4. The flow process for MRI classification.

and useful feature set from the preprocessed breast DCE-MRI scans. These features include enhanced Legendre polynomial (ELP) features, kinetic features, and deep learning features.

A. Enhanced Legendre polynomial (ELP) features extraction

This study develops a new handcrafted feature extraction method based on the Enhanced Legendre Polynomial (ELP). Image texture is an essential component of many medical image analyses and has a significant positive impact on the classification of breast images. Because of its abilities to identify pixels and edges in an image, polynomials are important in image processing. Variations in image intensity values can be identified by polynomial-based image feature extraction. Legendre polynomials can represent features in a way that reduces redundancy because they are orthogonal over a given interval. This characteristic is especially helpful in image processing because it makes it easier to effectively capture an image's key elements without causing overlap. These polynomials, which provide solutions to Legendre's differential equation, are extensively employed in a broad range of mathematical and practical contexts, especially in spherical harmonics-related issues and Laplace equation solving. Numerous studies and tabulations have been conducted on these zeros. The Legendre zeros are real for even degrees and appear in complex conjugate pairs for odd degrees. They are symmetric regarding the origin. As

$$\eta_{\nu,k} = \left(1 - \frac{1}{8\nu^2} + \frac{1}{8\nu^3}\right) \cos\left(\pi \frac{4k-1}{4\nu+2}\right) \quad (1)$$

the Legendre zeros are represented, where n is the Legendre polynomial's degree and k is an index that ranges from $1 \rightarrow \nu$, signifying the k -th zero of the ν -th Legendre polynomial [38]. The Legendre zeros are frequently employed in mathematical analysis and computing methods, particularly when dealing with boundary value and integral equation issues. From a mathematical standpoint, assume that an image \mathcal{I} in a usual state is a matrix $n \times m$ dimension. It is often assumed that $Y_{n \times m} = Y_n \times Y_m$ where

$$Y_\nu^k := (\eta_{\nu,k} : k = 1, \dots, \nu) \subset (-1, 1),$$

Such that

$$Y_\nu^k = \left(\left(1 - \frac{1}{8\nu^2} + \frac{1}{8\nu^3}\right) \cos\left(\pi \frac{4k-1}{4\nu+2}\right) : k = 1, \dots, \nu \right) \subset (-1, 1) \quad (2)$$

and

$$\lim_{\nu \rightarrow 1} \left(1 - \frac{1}{8\nu^2} + \frac{1}{8\nu^3}\right) \cos\left(\pi \frac{4k-1}{4\nu+2}\right) = \cos\left(\frac{1}{6}(4k-1)\pi\right) := \cos(\tau_k) \quad (3)$$

Assume that

$$Y_{n \times m} = ((\eta_i, \eta_j) : i = 1, \dots, n, j = 1, \dots, m), \quad n, m \in \mathbb{N}, k = 1. \quad (4)$$

Then the digital image of (n, m) pixels, can be described in terms of a continuous function Φ , as follows:

$$\mathcal{I}_{ij} := \Phi(Y_{n \times m}) = \Phi(\eta_i, \eta_j), \quad i = 1, \dots, n, j = 1, \dots, m. \quad (5)$$

Suppose that $\widetilde{\mathcal{I}}_{ij}$ is the actual, somewhat tainted version of the data that is accessible as input satisfying.

$$\widetilde{\mathcal{I}}_{ij} = \widetilde{\Phi}(Y_{n \times m}) = \widetilde{\Phi}(\eta_i, \eta_j), \quad i = 1, \dots, n, j = 1, \dots, m. \quad (6)$$

The goal of the feature extraction issue is to discover a fair approximation of the resampled image $[\mathcal{I}_{ij}]_{res}$, which is composed of samples of Φ at various (more or less dense) grid points ($Y_{n \times m}$), beginning from the input data $[\mathcal{I}_{ij}]_{in}$. To continue, with the following approximation applied:

$$\Lambda_{n,m} \widetilde{\Phi}(Y_{n \times m}) := \sum_{i=1}^n \sum_{j=1}^m \widetilde{\Phi}(\eta_i, \eta_j) \gamma_i \gamma_j, \quad (7)$$

where γ_i and γ_j are the Polya-Schur-Legendre multipliers satisfying the relation [39,40]

$$\gamma_i^2 - \gamma_{i-1} \gamma_{i+1} \geq 0, \quad \gamma_i \leq \gamma_{i+1} \quad i \in \mathbb{N}. \quad (8)$$

In [40]-Proposition 3 shows that γ_i has a quadratic formula

$$\gamma_i = i^2 + \alpha i + \beta, \quad 0 \leq \beta \leq \frac{1}{4}(1 + \alpha)^2, \quad \alpha \geq -1. \quad (9)$$

For some fixed values of α and β ,

$$\Lambda_{n,m} \widetilde{\Phi}(Y_{n \times m}) \rightarrow \widetilde{\Phi}(Y_{n \times m}) = \widetilde{\Phi}(\eta_i, \eta_j) = [\mathcal{I}_{ij}]_{in}, \quad i = 1, \dots, n, j = 1, \dots, m. \quad (10)$$

The proposed approach consists of samples that include these polynomials. Thus, the recommended technique calculates the matrix

$$[\mathcal{I}_{ij}]_{out} = \Lambda_{n,m} \widetilde{\Phi}(Y_{n \times m}) = \sum_{i=1}^n \sum_{j=1}^m \widetilde{\Phi}(\eta_i, \eta_j) \gamma_i \gamma_j. \quad (11)$$

Combining the above equations (the input and output of data),

$$[\mathcal{I}_{ij}]_{out} = \sum_{i=1}^n \sum_{j=1}^m [\mathcal{I}_{ij}]_{in} \gamma_i \gamma_j, \quad i = 1, \dots, n, j = 1, \dots, m. \quad (12)$$

where

$$\gamma_i = \gamma(\eta_i) = \eta_i^2 + \alpha \eta_i + \beta, \quad 0 \leq \beta \leq \frac{1}{4}(1 + \alpha)^2, \quad \alpha \geq -1.$$

And

$$\gamma_j = \gamma(\eta_j) = \eta_j^2 + \alpha \eta_j + \beta, \quad 0 \leq \beta \leq \frac{1}{4}(1 + \alpha)^2, \quad \alpha \geq -1.$$

From (3), the structure formula is as follows:

$$[\mathcal{I}_{ij}]_{out} = \sum_{i=1}^n \sum_{j=1}^m [\mathcal{I}_{ij}]_{in} (\eta_{ij}^2 + \alpha \eta_{ij} + \beta), \quad i = 1, \dots, n, j = 1, \dots, m. \quad (13)$$

Where η represents the probability of the pixel. A value of 0.8 was selected experimentally for α and $\beta = 0.81$ is determined empirically based on α .

The first step in the feature extraction process is to divide the images into 16x16 pixel non-overlapping blocks. Next, each block's texture features are extracted. After extracting the texture features from each image using Eq. (13), the dimensionality reduction of features is applied. This guarantees that the algorithm is working at its most effective and efficient configurations. The measures of "Mean", "Variance", "Skewness", and "Kurtosis" are used in the current study to reduce the dimensionality of the extracted data in each image. The "Mean" for features F of M scalar observations is defined as

$$Mn = \frac{1}{M} \sum_{i=1}^M F_i \quad (14)$$

The definition of a "Variance" is

$$Vc = \frac{1}{M-1} \sum_{i=1}^{NM} |F_i - \mu|^2 \quad (15)$$

where μ is the "Mean" of F_i

The Skewness, a measurement of the asymmetry of the feature data around the feature mean, is defined as

$$Ss = \frac{V(x - \mu)^3}{\sigma^3} \quad (16)$$

The variable $V(t)$ denotes the estimated value of the quantity t , while σ stands for the “standard deviation.” As “Kurtosis” is defined,

$$Ks = \frac{V(x - \mu)^4}{\sigma^4} \quad (17)$$

The definition of the “Standard deviation” is

$$St = \sqrt{\frac{1}{M-1} \sum_{i=1}^M |F_i - \mu|^2} \quad (18)$$

To demonstrate the efficacy of the proposed ELP in identifying distinguishing features from breast images, Fig. 5, presents the feature distribution as a quantitative foundation for feature separation.

B. Kinetic features

The time-signal intensity curve (TIC) that is determined from DCE-MRI, reflects the hemodynamic features of the breast lesion over time. Where the pattern of variation in the signal intensity following the injection depends on the vascularization and the tissue's ability to withstand the contrast agent [41]. Where, it is further analyzed to provide several important parametric parameters that are useful for breast diagnosis, such as signal intensity slope (SI_{slope}), maximum signal intensity (MSI), initial enhancement ($E_{Initial}$), the peak enhancement (E_{Peak}), early signal enhancement ratio (ESER), second enhancement (SEP), and the gradient (θ) [4,6,8,42].

C. Conventional CNN feature extraction

The kinetic features were created with expert knowledge, but despite this, they have very high sensitivity but relatively low specificity for identifying breast lesions because ductal and lobular masses share similar characteristics. This leads to an increase in false positive cases and needless biopsies [1,43,44]. Therefore, to identify the most discriminating characteristics in breast lesions, a learning-based method is required to extract high-level features with high specificity using deep learning. The deep features are extracted from the consecutive sequences (t_0 , t_1 , t_2 , and t_3) of DCE-MRI after cropping breast lesions manually by an experienced radiologist and padding the cropped images from margins with zeros to standardize all cropped images to 98×109

pixels prior to implementation of the CNN. The CNN architecture consists of several building blocks, such as convolution layers, pooling layers, and fully connected layers. Where, a typical proposed architecture CNN includes a set of repetitions of a stack of several convolution layers and a pooling layer, followed by one fully connected layer. The DCE-MRI slices are transformed into the desired output through these layers. Each convolutional layer includes a sliding multiplication and addition of regional data points of DCE-MRI by a small array of numbers called kernel filters. Where, these kernel filters are shifted from one position to another by a specific number of pixels, called stride. By using sets of different kernels a set of regional feature maps is produced, then rectified by eliminating all negative numbers by using ReLU activation function, and rectified through the pooling layer for down sampling the spatial domain of input image to reduce computation [6,8]. To regularize the training process of CNN, the feature maps are normalized by using a batch normalization layer. Finally, CNN works by applying a series of convolution and pooling layers to the provided DCE-MRI slices, and simultaneously, the network's weights are updated to reduce the error function by using the gradient-based optimization algorithm. Fig. 6 shows the proposed CNN structure of extracting deep features (DFs) from the breast DCE-MRI sequences, where the same network is repeatedly used to extract deep features from dynamic pre- and post-contrast respectively. Consequently, two (DFs) are extracted from each time phase of the breast DCE-MRI sequence.

An additional technique for visualizing the contribution of extracted features is the Shapley explanation graph, which shows how extracted features influence a model's predictions. Shapley explanation graph clarifies the relative contributions of each feature to a prediction for a particular instance in the context of machine learning. The length of the bars indicates the size of the contribution, it assists in identifying which features are significant and showing the average influence of each feature on the model's predictions. The x-axis illustrates the mean absolute SHAP values, representing the average magnitude of a feature's impact on the predictions, while the y-axis illustrates the feature names. It is evident from the analysis of the Shapley graphs in Fig. 7, that x5 and

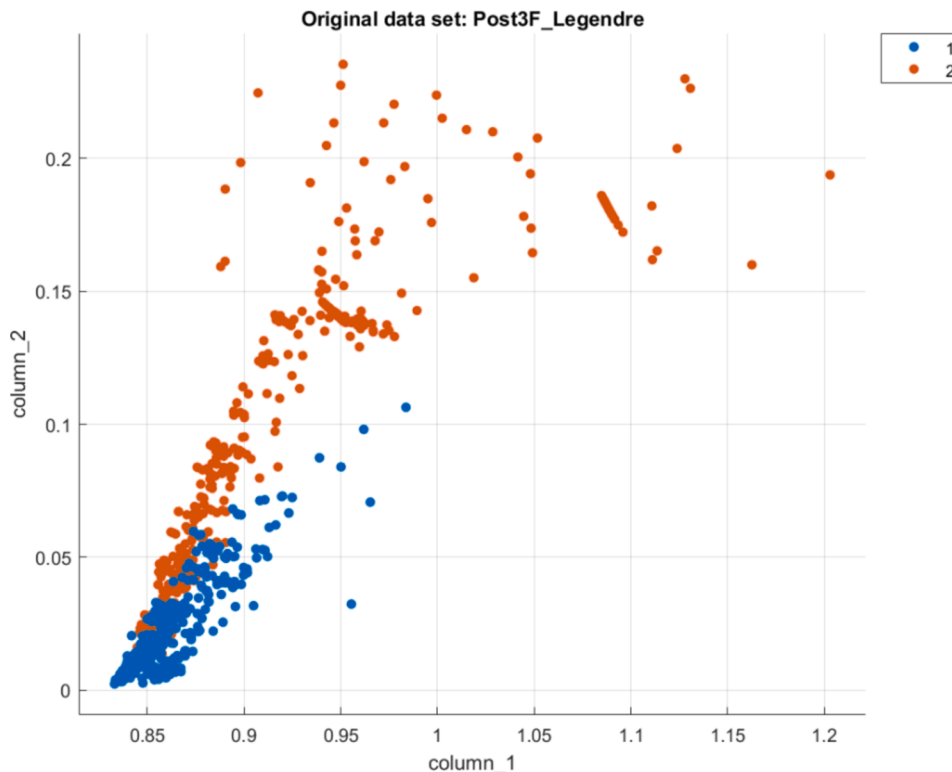


Fig. 5. The two classes' distribution features: Lobular Pre (Blue), and Ductal Pre (red).

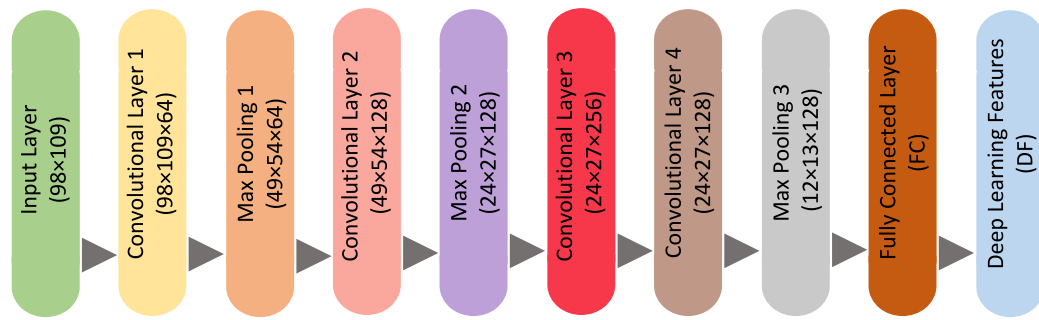


Fig. 6. Structure of DF extraction.

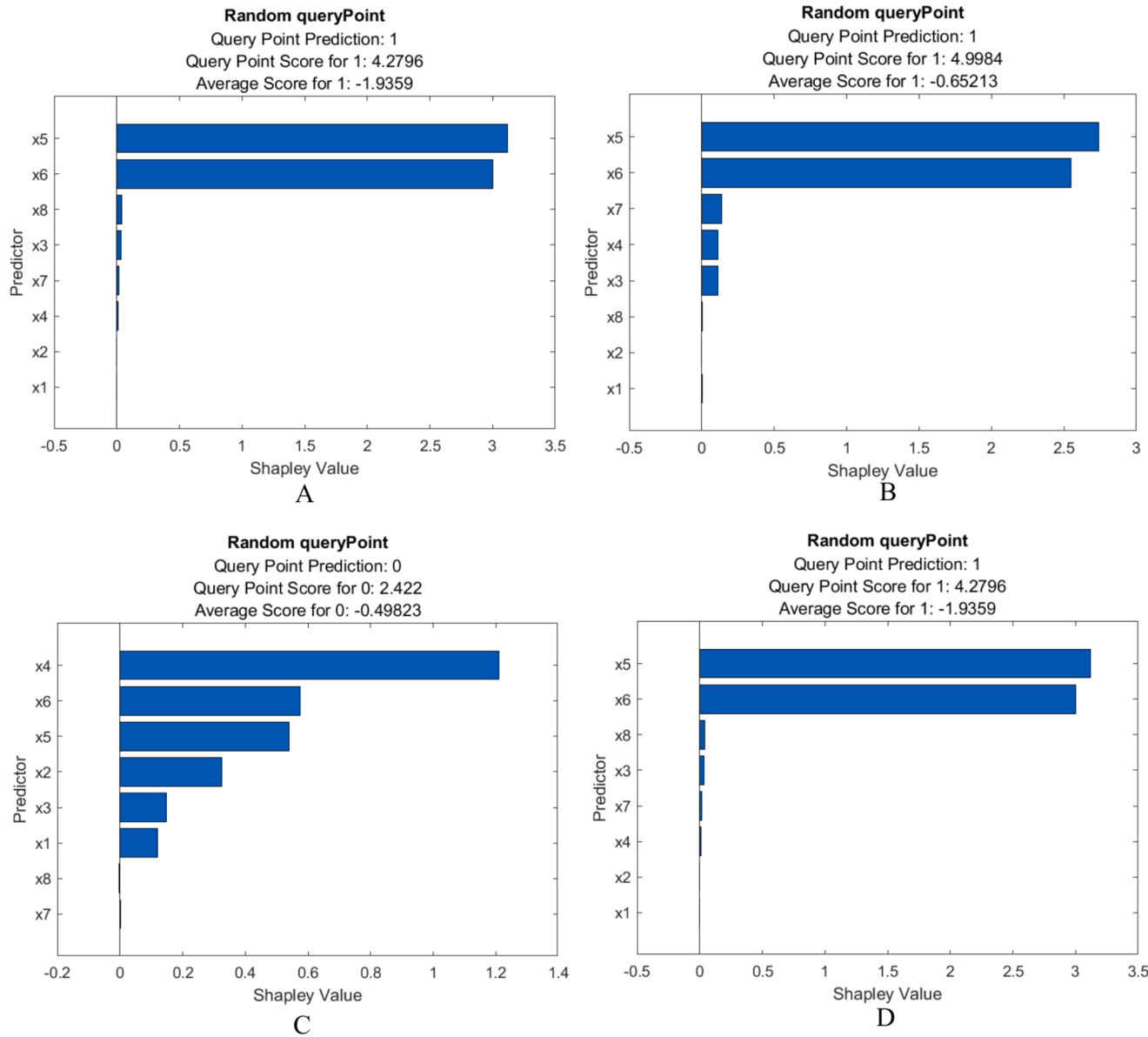


Fig. 7. The Shapley summary, A) Pre-contrast features, B) Post1-contrast features, C) Post2-contrast features, and D) Post3-contrast features.

x6 have the highest mean absolute SHAP value in pre-contrast (A), post 1-contrast (B) and post 3-contrast dynamics(D), making them the most significant features in the model. While features x1 to x6 represent a good performance in Post 2-contrast dynamic(C). However, the relatively smaller impacts of features x8 and x7 indicate that they might not

be as important to the model's predictions.

4. Results and discussion

The experimental results show that when all features were

combined, the classification of breast DCE-MRI into ductal and lobular masses achieved the best performance. In this study, each time phase of breast DCE-MRI (t_0 , t_1 , t_2 , and t_3) has a feature vector consisting of 6 features (2 and 4 features from the CNN and ELP methods, respectively). Additionally, 10 kinetic features were extracted from each breast DCE-MRI sequence. In total, 34 features were included in the feature vector, extracted from the four-time phases of the breast DCE-MRI sequence. MATLAB 2024a was utilized for the execution of each test. This study uses the 5-fold cross-validation technique. The dataset is divided evenly into five subsets, where one-fold (20 % of the data) is used for testing while the remaining four folds (80 % of the data) are used for training. These five subsets are used independently to produce five different classification results with completely different testing and training samples at each time, as shown in Fig. 8. According to this scheme, the overall test result is obtained from averaging these five different classification results.

In this study, an experimental initialization of the proposed CNN architecture for the identification of ductal and lobular breast masses in DCE-MRI scans was conducted. Table 1 provides an overview of its nine layers. It was trained with 0.9 momentum, 0.0001 learning rate, 20 maximum epochs, a batch size of 64, and 100 maximum iterations for each layer for all experiments. The training progress plots of CNNs of four-time phases of breast DCE-MRI emphasize that the proposed CNN network demonstrates superior performance in extracting DF from breast DCE-MRI scans, as shown in Fig. 9.

The experimental results indicate that the extracted ELPs features, when combined with kinetic and DF features and classified by a SVM model, enhanced the effectiveness of diagnosing breast DCE-MRI sequences into ductal and lobular breast masses. Where, it is noted that the performance of distinguishing between ductal and lobular breast masses was significantly improved when combining the kinetic feature that are extracted by time-intensity-curve (TIC) analysis and DF features with the proposed ELPs features, surpassing their performance when using them separately, as demonstrated in Table 2. Where, the highest accuracy of 97.99 % was achieved at t_1 of delayed post-contrast imaging when applying the SVM classifier to the combined extracted features as shown in Fig. 10.

Furthermore, the receiver operating characteristic (ROC) curves for the classification performance of the extracted features on the testing set as shown in Fig. 11. The model's capacity to differentiate between classes using the probabilities produced by the SVM classifier was summarized by the ROC curves that were extracted during the testing phase. The curve provides a final evaluation of the model's generalization ability by reflecting its performance on an entirely unknown test set.

The utilized gadolinium-based contrast agents (GBCA) with MRI scans includes number of side effects such as injection site pain, nausea, itching, rash, dizziness, headaches and hypersensitivity reactions, thyroid dysfunction, and contrast-induced nephropathy [45,46].

Although, the first timing of delayed post-contrast imaging (t_1) had the highest accuracy among all DCE-MRI phases in all feature extraction methods, the pre-contrast phase achieved the second-highest accuracy of 97.63 and was the closest in performance to the t_1 phase. Thus, it is possible to use the pre-contrast to distinguish the breast ductal and lobular masses instead of using GBCA material especially in patients with severe chronic kidney disease.

The advantages of combining the deep learning feature extraction,

Table 1
Proposed architecture of CNN.

Layer Name	Kernel filter	Kernel Size	Feature Map
Input Layer		(98 × 109)	
Convolutional layer 1	64	(3 × 3)	(98 × 109 × 64)
Pooling layer 1		(2 × 2)	(49 × 54 × 64)
Convolutional layer 2	128	(3 × 3)	(49 × 54 × 128)
Pooling layer 2		(2 × 2)	(24 × 27 × 128)
Convolutional layer 3	256	(3 × 3)	(24 × 27 × 256)
Convolutional layer 4	128	(3 × 3)	(24 × 27 × 128)
Pooling layer 3		(2 × 2)	(12 × 13 × 128)
Fully connected layer		(1 × 2)	(1 × 2)

kinetic features, and enhanced Legendre polynomial features in hybrid approach feature extraction, improved the accuracy of breast cancer detection as well as improved classification performance by capturing distinct facets of the data, resulting in a more thorough depiction of the underlying patterns. Combining these features ensured that no crucial details were missed, including both high-level and low-level features.

4.1. Ablation study

In an ablation study, we investigate the performance of the proposed model by removing certain components to understand their contribution to the overall model. First, an ablation analysis was conducted through five experiments that included altering the number of kernel filters to assess their impact on the performance of the proposed network, as illustrated in Table 3. Furthermore, another ablation analysis was performed by implementing three experiments that measured the effect of altering the preprocessing algorithms on the proposed model, as demonstrated in Table 4.

4.2. Comparison with existing state-of-the art

Several prior studies that examined the diagnosis of breast DCE-MRI breast scans were compiled in Table 5 to verify the efficacy of the suggested approach. Maiti, Nayak [27] investigated the radiomic features that were extracted from DCE-MRI for distinguishing between IDC and ILC breast cancers. The authors achieved an AUC of 99.8 % on a dataset that included (30 IDC and 28 ILC). Faraz, Dauce [29] extracted four features sets by different methods from 420 DCE-MRI images, the achieved AUC was 73 %. Moreover, the radiomic features was also used by Conte, Tafuri [30], on only (11 ILC and 44 IDC) and their achieved AUC was 70 %.

The proposed study was successful in discriminating IDC and ILC breast cancer, with a detection accuracy and AUC of 97.99 % and 100 % respectively. In this study, the hybrid features of the DCE-MRI images which included kinetic, deep, and ELP features were taken from a publicly accessible dataset. The textural extraction feature based on polynomials are the most significant since they can detect small changes in image intensity values precisely.

5. Conclusion

This study presented a new method for automatically differentiating between ILC and IDC breast masses, providing accurate diagnosis and

	Fold 1	Fold 2	Fold 3	Fold 4	Fold 5	
Experiment 1	Training Data		Testing Data			
Experiment 2	Training Data		Testing Data	Training Data		
Experiment 3	Training Data		Testing Data	Training Data		
Experiment 4	Training Data	Testing Data	Training Data			
Experiment 5	Testing Data	Training Data				

- Test 1
- Test 2
- Test 3
- Test 4
- Test 5

Fig. 8. Implementation of experimental results.

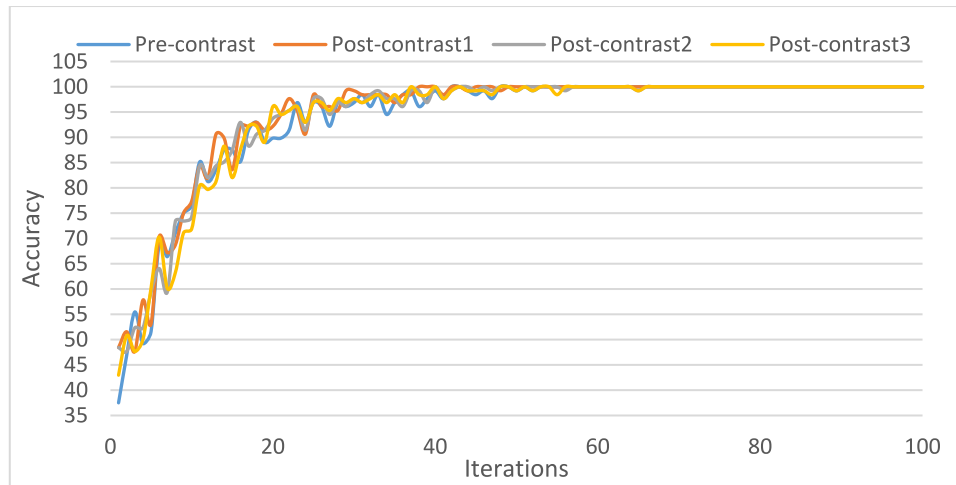


Fig. 9. The training plots of the proposed CNN of four-time phases of breast DCE-MRI.

Table 2

Achieved results by combining the proposed ELP with and without kinetic and CNN features using SVM classifier.

Features	ACC 100%	TP 100%	TN 100%	Sensitivity 100%	Specificity 100%	AUC 100%
Kinetic features	87.80	93.34	80.58	86.08	90.40	87
ELP Pre-contrast	95.25	96.27	93.95	95.34	95.14	96
ELP Post-contrast 1	95.43	96.43	94.15	95.50	95.35	96
ELP Post-contrast 2	93.61	94.97	91.86	93.75	93.42	95
ELP Post-contrast 3	93.88	95.45	91.86	93.78	94.02	95
DF Pre-contrast	96.35	94.97	98.12	98.48	93.81	97
DF Post-contrast 1	96.62	94.97	98.75	98.98	93.85	97
DF Post-contrast 2	95.98	94.48	97.91	98.31	93.24	96
DF Post-contrast 3	94.98	94.16	96.03	96.83	92.74	98
Combined Pre-contrast	97.63	96.75	98.75	99.00	95.94	100
Combined Post-contrast 1	97.99	97.40	98.75	99.01	96.73	100
Combined Post-contrast 2	96.80	96.10	97.70	98.18	95.12	97
Combined Post-contrast 3	95.80	95.45	96.24	97.03	94.27	96

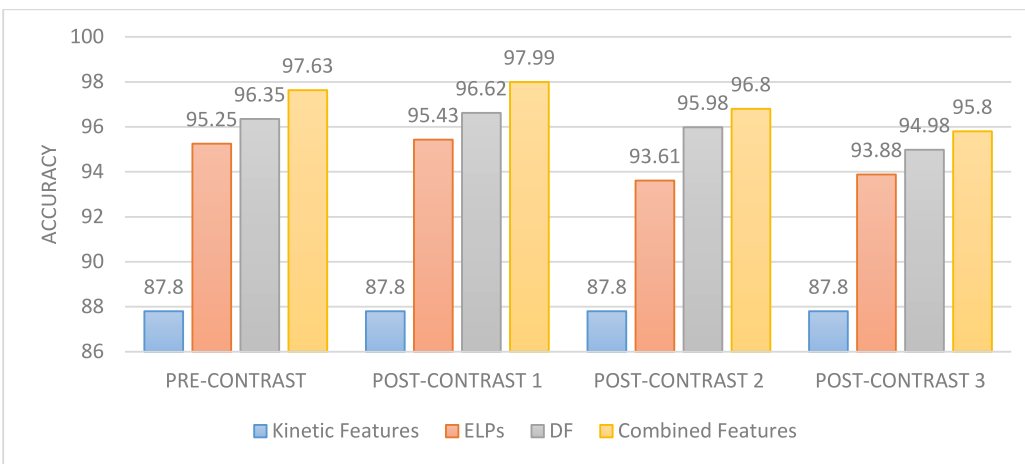


Fig. 10. Comparison of CNN, Kinetic, ELPs, and combined features for the classification of breast lesions in four different DCE-MRI sequences.

guiding efficient treatment that can lower the risks of bleeding and infection. In this study, three features extraction methods were used to enhance the automatic discrimination of ILC and IDC breast masses. The texture image features were extracted by the proposed ELP model in

regions with high and low gray-level variation. The kinetic features were extracted after being analyzed by radiologists, and the deep learning features extraction were applied to improve the automatic discrimination of ILC and IDC breast masses. The combination of these three

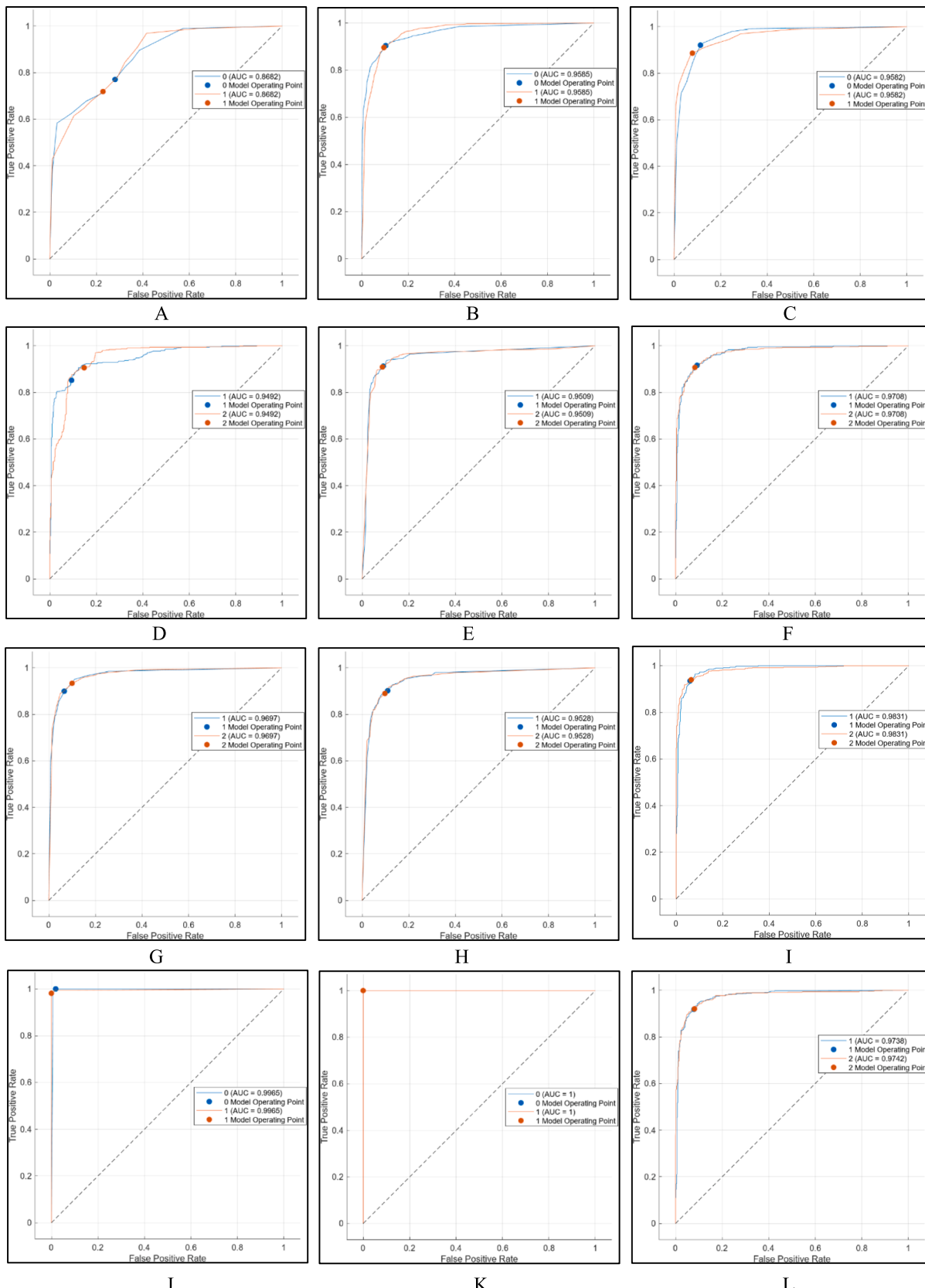


Fig. 11. ROC curves for the classification performance, A) Kinetic features, B) ELP Pre-contrast, C) ELP Post-contrast 1, D) ELP Post-contrast 2, E) ELP Post-contrast 3, F) DF Pre-contrast, G) DF Post-contrast 1, H) DF Post-contrast 2, I) DF Post-contrast 3, J) Combined Features of Pre-contrast, K) Combined Features of Post 1-contrast, L) Combined Features of Post 2-contrast, M) Combined Features of Post 3-contrast.

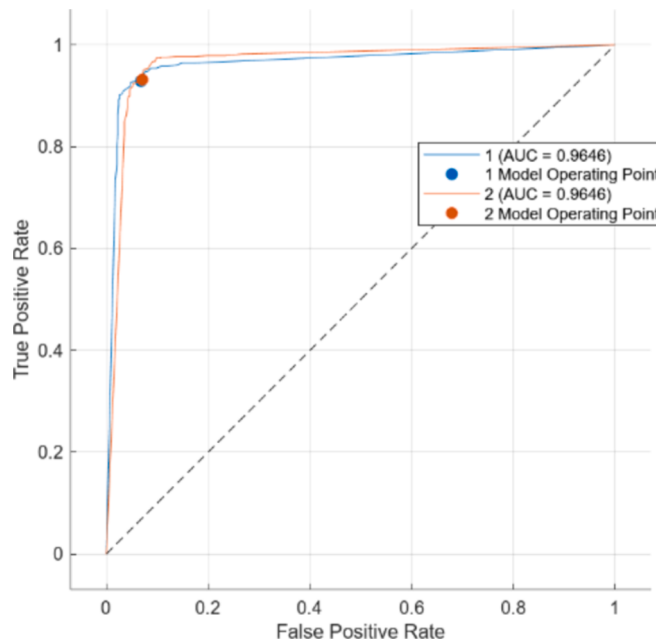


Fig. 11. (continued).

Table 3
Ablation study.

Experiment	Kernel filter (convolutional layer _{1, 2, 3, and 4})	Accuracy
Ablation study 1	32, 64, 128 and 64	94.90
Ablation study 2	32, 128, 128 and 64	95.12
Ablation study 3	32, 256, 128 and 64	95.44
Ablation study 4	64, 256, 128 and 64	96.22
Ablation study 5	64, 256, 128 and 128	96.89
Proposed model	64, 128, 256 and 128	97.99

Table 4
Ablation study.

Experiment	Preprocessing algorithms	Accuracy
Ablation study 1	None	92.33
Ablation study 2	Enhancement	93.10
Ablation study 3	Normalization	94.31
Ablation study 4	Registration	94.11
Ablation study 5	Enhancement and normalization	96.14
Ablation study 6	Enhancement and registration	96.32
Proposed model	Enhancement, normalization, and registration	97.99

features methods was the novelty of this study. The results revealed that using the hybrid features improved the detection accuracy to 97.99 % in combined post-contrast 1. The findings provided an important development in the automated discrimination of invasive ILC and IDC breast masses as well as lowers misdiagnosis rates and gives clinicians a strong tool for confirming diagnoses, especially in cases that are unclear. Furthermore, utilizing larger datasets with multimodal imaging integration be considered in the future work to improve differentiation accuracy.

CRediT authorship contribution statement

Ali M. Hasan: Writing – original draft, Software, Methodology. **Noor K.N. Al-Waely:** Data curation. **Hadeel K. Aljobouri:** Software, Formal analysis. **Hamid A. Jalab:** Writing – review & editing, Methodology. **Rabha W. Ibrahim:** Methodology, Investigation. **Farid Meziane:** Writing – review & editing, Supervision.

Table 5
Comparisons of the proposed model to other breast DCE-MRI diagnosis methods.

Refs.	Dataset	Features	Classifier	Accuracy	AUC
Maiti, Nayak [27]	Dukes breast cancer MRI dataset (30 IDC and 28 ILC)	- GLDM - GLCM - First order - GLRLM - GLSZM - NGTDM	Statistical classifier	–	99.8 %
Faraz, Daucé [29]	420 MR images	- GLCM - GLRLM - NGTDM - GLSZM	SVM	–	73.0 %
Conte, Tafuri [30]	55 anonymized DCE-MRI sequences (11 ILC and 44 IDC)	- GLCM - First order - GLRLM - GLDM - GLSZM	SVM	–	70.0 %
Proposed	430 DCE-MRI (616 IDC and 479 ILC)	- ELP features - Kinetic features - DF features	SVM	97.99 %	100 %

Declaration of competing interest

The authors declare that they have no known competing financial interests or personal relationships that could have appeared to influence the work reported in this paper.

Acknowledgement

This study was supported by Al-Nahrain University, project (CMPMP-22-001), Iraq.

Data availability

Data will be made available on request.

References

- [1] A.M. Hasan, et al., Breast Cancer MRI Classification Based on Fractional Entropy Image Enhancement and Deep Feature Extraction, *Baghdad Sci. J.* (2022) 0221.
- [2] M.M.Y. Al-Hashimi, Trends in Breast Cancer Incidence in Iraq During the Period 2000–2019, *Asian Pac. J. Cancer Prev.* 22 (12) (2021) 3889–3896.
- [3] N.A. Al Alwan, General Oncology Care in Iraq, in: *Cancer in the Arab World*, Springer, Singapore, 2022, pp. 63–82.
- [4] A.M. Hasan, et al., A classification model of breast masses in DCE-MRI using kinetic curves features with quantum-Raina's polynomial based fusion, *Biomed. Signal Process. Control* 84 (2023) 105002.
- [5] A. Gabriel, G.P. Maxwell, Anatomy of the Breast, in: M.B. Calobraccio (Ed.), *Augmentation Mastopexy: Mastering the Art in the Management of the Ptotic Breast*, Springer International Publishing, Cham, 2020, pp. 1–10.
- [6] A.M. Hasan, et al., Diagnosis of breast cancer based on hybrid features extraction in dynamic contrast enhanced magnetic resonance imaging, *Neural Comput. & Applic.* (2023) 1–14.
- [7] G. Cserni, Histological type and typing of breast carcinomas and the WHO classification changes over time, *Pathologica* 112 (1) (2020) 25.
- [8] A.M. Hasan, et al., Molecular subtypes classification of breast cancer in DCE-MRI using deep features, *Expert Syst. Appl.* 236 (2024) 121371.
- [9] Makki, J., Diversity of breast carcinoma: histological subtypes and clinical relevance. Clinical medicine insights: Pathology, 2015. 8: p. CPath. S31563.
- [10] S.R. Hilal, H.S. Hasan, A.M. Hasan, Magnetic Resonance Imaging Breast Scan Classification based on Texture Features and Long Short-Term Memory Model, *NeuroQuantology* 19 (7) (2021) 41.
- [11] S.R. Lakhani, et al., WHO Classification of Tumours of the, *Breast* (2012).
- [12] S.S. Sun, et al., Association between mammographic features and clinicopathological characteristics in invasive ductal carcinoma of breast cancer, *Mol Clin Oncol* 2 (4) (2014) 623–629.
- [13] R. Barroso-Sousa, O. Metzger-Filho, Differences between invasive lobular and invasive ductal carcinoma of the breast: results and therapeutic implications, *Ther Adv Med Oncol* 8 (4) (2016) 261–266.
- [14] Wang, L., Early diagnosis of breast cancer. *Sensors*, 2017. 17(7): p. 1572.
- [15] H.L. Chen, et al., Comparison of the sensitivity of mammography, ultrasound, magnetic resonance imaging and combinations of these imaging modalities for the detection of small (≤ 2 cm) breast cancer, *Medicine (Baltimore)* 100 (26) (2021) e26531.
- [16] R. Choe, et al., Differentiation of benign and malignant breast tumors by in-vivo three-dimensional parallel-plate diffuse optical tomography, *J. Biomed. Opt.* 14 (2) (2009) 024020.
- [17] Susan G. Komen. Findings on a Mammogram and Mammogram Results. 2024 [cited 2024 09.03.2024]; Available from: <https://www.komen.org/breast-cancer/screening/mammography/mammogram-images/>.
- [18] D. Zheng, X. He, J. Jing, Overview of Artificial Intelligence in Breast Cancer Medical Imaging, *J. Clin. Med.* 12 (2) (2023).
- [19] F. Gharekhloo, M.M. Haseli, S. Torabian, Value of Ultrasound in the Detection of Benign and Malignant Breast Diseases: A Diagnostic Accuracy Study, *Oman Med. J.* 33 (5) (2018) 380–386.
- [20] S. Radhakrishna, et al., Role of magnetic resonance imaging in breast cancer management, *South Asian J Cancer* 7 (2) (2018) 69–71.
- [21] A. Bagchi, P. Pramanik, R. Sarkar, A multi-stage approach to breast cancer classification using histopathology images, *Diagnostics* 13 (1) (2022) 126.
- [22] C. Gallego-Ortiz, A.L. Martel, Using quantitative features extracted from T2-weighted MRI to improve breast MRI computer-aided diagnosis (CAD), *PLoS One* 12 (11) (2017) e0187501.
- [23] R.M. Mann, N. Cho, L. Moy, Breast MRI: state of the art, *Radiology* 292 (3) (2019) 520–536.
- [24] Jansen, S.A., et al., Differentiation between benign and malignant breast lesions detected by bilateral dynamic contrast-enhanced MRI: a sensitivity and specificity study. *Magnetic Resonance in Medicine: An Official Journal of the International Society for Magnetic Resonance in Medicine*, 2008. 59(4): p. 747–754.
- [25] D.A. Bluemke, et al., Magnetic resonance imaging of the breast prior to biopsy, *J. Am. Med. Assoc.* 292 (22) (2004) 2735–2742.
- [26] Clinic, M. Breast biopsy. 2024; Available from: <https://www.mayoclinic.org/tests-procedures/breast-biopsy/about/pac-20384812>.
- [27] S. Maiti, et al., Differentiation of invasive ductal and lobular carcinoma of the breast using MRI radiomic features: a pilot study, *F1000Res* 13 (2024) 91.
- [28] A. Saha, et al., A machine learning approach to radiogenomics of breast cancer: a study of 922 subjects and 529 DCE-MRI features, *Br. J. Cancer* 119 (4) (2018) 508–516.
- [29] K. Faraz, et al., Characterization of Breast Tumors from MR Images Using Radiomics and Machine Learning Approaches, *Journal of Personalized Medicine* 13 (7) (2023) 1062.
- [30] L. Conte, et al., Breast Cancer Mass Detection in DCE-MRI Using Deep-Learning Features Followed by Discrimination of Infiltrative vs. In Situ Carcinoma through a Machine-Learning Approach, *Appl. Sci.* 10 (17) (2020) 6109.
- [31] Hasan, A.M., et al. MRI brain scan classification using novel 3-D statistical features. in Proceedings of the Second International Conference on Internet of things, Data and Cloud Computing. 2017. ACM.
- [32] V.R. Tripathi, M.N. Tibdewal, R. Mishra, A survey on Motion Artifact Correction in Magnetic Resonance Imaging for Improved Diagnostics, *SN Comput. Sci.* 5 (3) (2024) 281.
- [33] T.B. Smith, MRI artifacts and correction strategies, *Imaging in Medicine* 2 (4) (2010) 445.
- [34] N.B. Khalaf, et al., Simplified Convolutional Neural Network Model for Automatic Classification of Retinal Diseases from Optical Coherence Tomography Images, *Al-Nahrain Journal for Engineering Sciences* 26 (4) (2023) 314–319.
- [35] A. Hasan, F. Meziane, Automated screening of MRI brain scanning using grey level statistics, *Comput. Electr. Eng.* 53 (2016) 276–291.
- [36] A. Carré, et al., Standardization of brain MR images across machines and protocols: bridging the gap for MRI-based radiomics, *Sci. Rep.* 10 (1) (2020) 12340.
- [37] M.H. Hasan, H.S. Hasan, A.M. Hasan, MRI Brain Scans Classification Using Bi-directional Modified Gray Level Co-occurrence Matrix and Long Short-Term Memory, *NeuroQuantology* 18 (9) (2020) 54.
- [38] G.H. Golub, J.H. Welsch, Calculation of Gauss quadrature rules, *Math. Comput.* 23 (106) (1969) 221–230.
- [39] Schur, J. and G. Plya, Über zwei Arten von Faktorenfolgen in der Theorie der algebraischen Gleichungen. 1914.
- [40] K. Blakeman, et al., On Legendre multiplier sequences, *Missouri J. Math. Sci.* 24 (1) (2012) 7–23.
- [41] C. Lavini, M.S. Buitier, M. Maas, Use of dynamic contrast enhanced time intensity curve shape analysis in MRI: theory and practice, *Rep. Med. Imaging* (2013) 71–82.
- [42] C. Lavini, M.S. Buitier, M. Maas, Use of dynamic contrast enhanced time intensity curve shape analysis in MRI: theory and practice, *Rep. Med. Imaging* 6 (2013) 71–82.
- [43] S.-N. Yang, et al., Kinetic curve type assessment for classification of breast lesions using dynamic contrast-enhanced MR imaging, *PLoS One* 11 (4) (2016) e0152827.
- [44] H. Alrubaie, et al., Convolutional Neural Network Deep Learning Model for Improved Ultrasound Breast Tumor Classification, *Al-Nahrain Journal for Engineering Sciences* 26 (2) (2023) 57–62.
- [45] M. Andreucci, R. Solomon, A. Tasanarong, Side effects of radiographic contrast media: pathogenesis, risk factors, and prevention, *Biomed Res. Int.* 2014 (1) (2014) 741018.
- [46] M. Andreucci, R. Solomon, A. Tasanarong, Side effects of radiographic contrast media: pathogenesis, risk factors, and prevention, *Biomed Res. Int.* 2014 (2014) 741018.